Article

Mineralogical and Geochemical Characteristics of the H-Pit of the Chatree Gold Deposit, Central Thailand: A Case Study for Assessment of Acid Rock Drainage and Heavy Metal Sources

Sirawit Kaewpaluk [1], **Abhisit Salam** [1,*], **Thitiphan Assawincharoenkij** [1,2,*], **Takayuki Manaka** [3], **Sopit Poompuang** [1] **and Surachat Munsamai** [4]

1 Department of Geology, Faculty of Science, Chulalongkorn University, Bangkok 10330, Thailand
2 Applied Mineral and Petrology of Special Task Force for Activating Research, Department of Geology, Faculty of Science, Chulalongkorn University, Bangkok 10330, Thailand
3 Institute for Geo-Resources and Environment, Geological Survey of Japan, National Institute of Advanced Industrial Science and Technology (AIST), Tsukuba 305-8567, Ibaraki, Japan
4 Akara Resources Public Company Limited, Phichit 66230, Thailand
* Correspondence: masoesalam@gmail.com (A.S.); thitiphan.a@chula.ac.th (T.A.)

Abstract: H-pit is one of the significant ore lenses of the Chatree mine in Thailand. Au-Ag mineralization mainly occurs as veins, stockworks, and minor breccias hosted by volcanic and volcaniclastic rocks. Disseminated pyrites are commonly present near mineralized veins in the hanging wall zone. This study aims to assess the acid rock drainage (ARD) potential and heavy metal content from the H-pit area. The results indicate that hanging wall rock is a potential acid-forming (PAF) material related to disseminated pyrite formed by hydrothermal alteration. In contrast, the footwall and ore zone materials are classified as non-acid forming (NAF). Because the ore zone has calcite in the veins, it may help buffer the material's acidity. The results of heavy metal analysis reveal that the ore zone has significantly higher contents of As, Cd, Cu, Pb, and Zn than those in the hanging wall and footwall zones. Moreover, the hanging wall and footwall materials have exceeding values for As, Cd, and Zn compared to those in typical igneous rocks. These heavy metals are interpreted to be sourced from (1) the primary composition in base metal sulfides (e.g., Cu, Pb, and Zn), (2) the substitution of trace elements in sulfides (e.g., As and Cd), and (3) the substitution of trace elements in calcite (e.g., Mn), as evidenced in the EPMA results. In conclusion, the hanging wall rocks in this study containing high sulfur in proximity to the ore zone are a PAF material with heavy metal contaminant sources, whereas the footwall and ore zone materials have a lower potential to be such sources at the Chatree mine.

Keywords: low-sulfidation epithermal; Au-Ag mineralization; sulfide minerals; acid rock drainage; heavy metals; environmental impact

1. Introduction

Ore mining has been concerned about the mine and local community issues of environmental pollution, particularly on water resources (e.g., surface and ground waters). These pollutions have potential long-term damage to the local environment and livelihood. In most cases, the pollution is principally caused by acid rock drainage (ARD) and/or acid mine drainage (AMD) [1–5]. ARD naturally occurs in altered and mineralized rocks producing acid, while AMD is acid production from sulfide materials generated by mining activity, i.e., waste rocks and tailings [6]. Another hazardous pollution is heavy metal contamination (e.g., As, Cd, Cr, Cu, Mn, Ni, Pb, Zn), generally caused by ARD/AMD as acidic water can promote metals leaching and removal in tailing medium [7–9].

Naturally, metallic mineral deposits contain abundant sulfide minerals, which potentially generate acid when decomposed due to oxidizing reactions [1,3,10]. Under acidic conditions, water in mining areas rapidly degrades waste rocks to release different amounts of heavy metals into the environment. Therefore, an understanding of mineralogical and geochemical characteristics can lead to a significant improvement in the upstream prevention of environmental impacts. Our study aims to identify and classify concerned materials, which is key to effective mine management to avoid causing environmental pollution [11]. Such a prediction study is suggested to be performed at the earliest exploration stage [3].

The Chatree Au-Ag mine in central Thailand is one of the largest gold mines in mainland SE Asia. The mineral resource of the Chatree deposit in 2016 is estimated to be 166.2 million tons at 0.66 g/t Au and 5.86 g/t Ag, containing 3.53 million ounces of gold and 31.3 million ounces of silver [12]. The gold mining operation at Chatree has produced approximately 1,500,000 ounces of gold since the operation was started in the early 2000s. However, the mining operation ceased at the end of 2016 by a particular order from the National Council for Peace and Order (NCPO) due to a dispute about environmental issues (i.e., heavy metals contaminant in water).

Several environmental studies have been undertaken at the Chatree mine area to assess potential AMD generation and heavy metal contamination in surface and ground waters, soil, tailing, and dumped waste rocks [8,13–17]. These studies conducted many tests on various waste and tailing materials and predicted potential environmental risks in the future in the mine area. However, these previous studies investigated only the downstream part of the mining operation (i.e., collecting samples from the waste dump and tailing site is the uppermost part of the stream). Thus, the studies could not identify sources of some materials with potential environmental risks at the mine. For example, Changul et al. [13] found that Mn content in tailing material is higher than the Thailand Soil Quality Standards, but they could not identify the source of the high Mn.

Therefore, this study assessed ore and host rock units with potential environmental risks in the future by describing and characterizing the geology and geochemistry of ore and host rocks at the H-pit. In addition, efforts are made to assume the sources of the predicted heavy metal contaminations. The H-pit is selected among several ore lenses (or pits) in the Chatree deposit, showing a distinct vertical zonation of footwall, ore, and hanging wall zones. Therefore, it may provide results between the different zones and thus allow us to identify sources of hazardous materials. Furthermore, it noted that all the geological data and samples used in this study are from previous materials created during the resource drilling exploration program around 10–20 years ago. Therefore, the results obtained in this study will demonstrate whether a reliable environmental assessment study can be performed even in the pre-mining exploration stage.

2. Geology of the Chatree Deposit

Thailand and its adjacent regions consist of two major tectonic terranes, including Sibumasu Terrane in the west and Indochina Terrane in the east (Figure 1a) [18–21]. The subduction and collision between the Sibumasu and Indochina Terranes occurred during the Permo–Triassic period. These resulted in the formation of two parallel volcano-plutonic belts along the western edge of the Indochina Terrane, namely Sukhothai Arc (or Sukhothai Fold Belt) and Loei Fold Belt [21–23]. The Loei Fold Belt (LFB) extends from Laos through northeastern Thailand (Loei province) and central Thailand (e.g., Phichit, Phetchabun, and Nakhon Sawan provinces) to eastern Thailand and western Cambodia (Figure 1a). This belt is the most important mineral belt in Thailand, especially for copper and gold resources. The significant copper and gold deposits of the belt include the Phu Lon (Cu-Au skarn) [24], Phuthep (Cu-Au skarn) [23,25], Phu Thap Fah (Au skarn) [26,27], Chatree (Au-Ag low-sulfidation epithermal) [28–33], Khao Phanom Pha (Au skarn) [21], Khao Lek (Fe-Cu skarn) [34], and French mine deposit (Cu-Au skarn) [35].
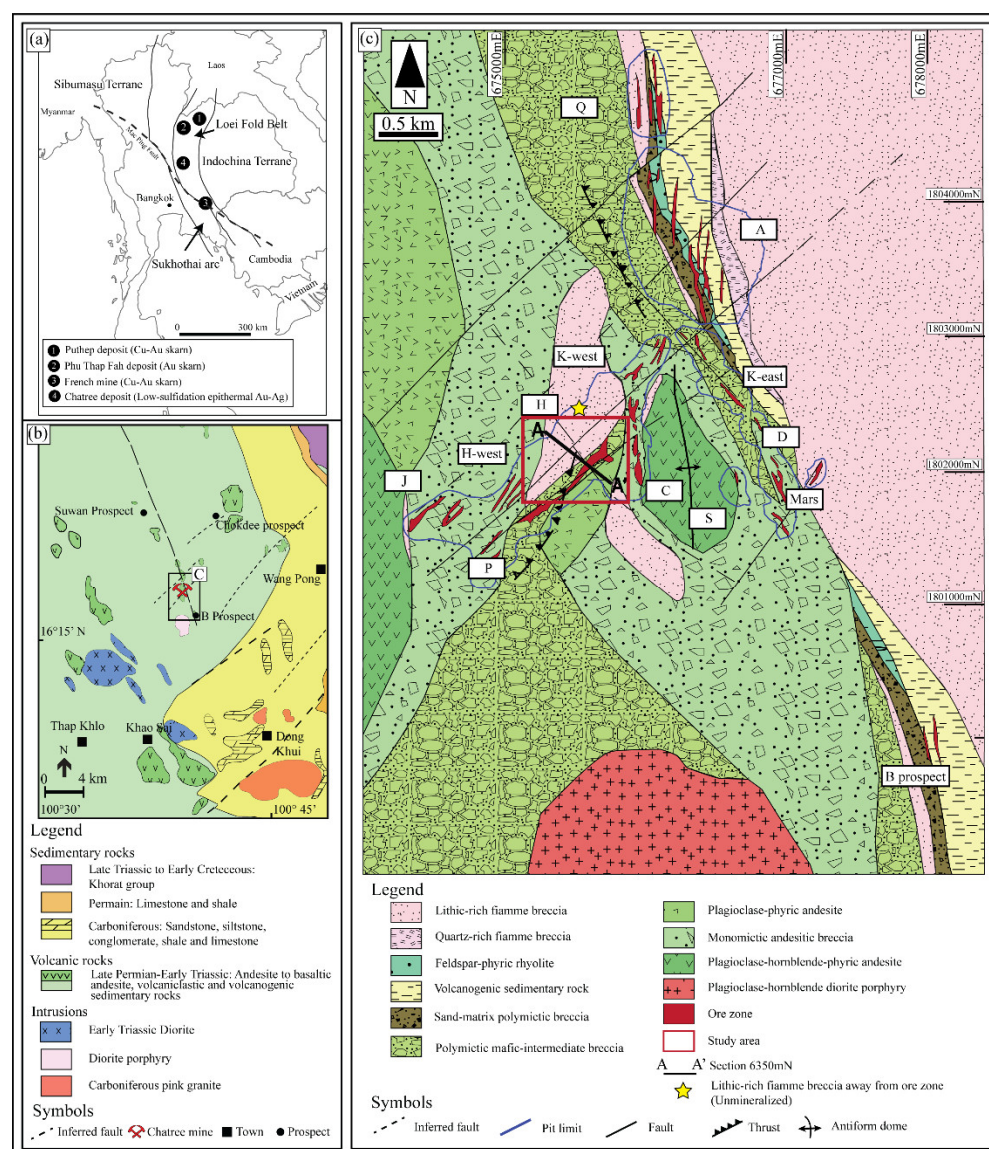
Figure 1. (**a**) Tectonic framework of Thailand and the surrounding regions, with locations of major Cu-Au deposits along the Loei Fold Belt. (**b**) District-scale geology of the Chatree deposit area. (**c**) Geological map of the Chatree deposit and the surrounding areas showing dominant volcanic and volcanogenic sedimentary rocks. The Chatree deposit has several pits, such as Q, A, K-west, K-east, H, C, H-west, J, P, D, S, and Mars pits. Data are modified after Salam [30]. The study focused on section 6350 mN and the lithic-rich fiamme breccia sample (background sample) collected away from the ore zone (yellow star).

The basement Carboniferous rocks and Permian limestone of the host rock sequence at the Chatree deposit are exposed in the eastern part of the deposit area. The host rock sequence at the Chatree deposit consists of volcanic and volcanogenic sedimentary rocks (Figure 1b,c). The Chatree volcanic sequence can be divided into four units from bottom to top as follows: porphyritic andesite unit, polymictic mafic-intermediate unit, volcanogenic sedimentary unit, and fiamme breccia unit [31]. The total thickness of the whole volcanic sequence is at least 550 m. The Late Triassic to Early Cretaceous Khorat Group covers the Chatree host volcanic rocks in the eastern part of the Chatree deposit area (Figure 1b). In addition, intrusive rocks in several different phases occur around the Chatree deposit area, including Carboniferous pink granite at Dong Khui, Early Triassic granite in the Wang Pong and Khao Rub Chang areas, and diorite Cu-Mo porphyry at the N prospect [30–32]. However, the diorite porphyry in the southern area isn't relevant to the

Chatree Au-Ag deposit because it has a younger mineralized age and a different origin of hydrothermal fluid [32].

The H ore lens is one of the main ore lenses at the Chatree deposit, and together with the nearby C ore lens, it (C-H ore lens) contains the mineral resource of 36.4 Mt @ 0.69 g/t Au and 4.0 g/t Ag in 2013 [36]. The main ore lenses at the Chatree deposit include the K-west, H, C, H-west, J, and P ore lenses that are hosted along the NE-SW fault zone, and the other NNW-SSE trending fault zone hosts the Q, A, K-east, D, Mars, and S ore lenses (Figure 1c). The H ore lens is characterized by the thickest ore zone (up to 100 m) among the ore lenses presenting along the NE-SW fault structure. The ore lenses become thinner at further southwestern (H-west, J, and P ore lenses) and northeastern (K-west and C ore lenses). At the K-west and C ore lenses, the NE-SW ore-hosting fault is truncated by the NNW-SSE fault, which also hosts ore lenses along the trend. Thus, it is interpreted as a syn- to post-mineralization structure (Figure 1c) [30].

3. Materials and Methods

3.1. Sample Collection, Petrographic Investigation, and EPMA Analysis

This study was conducted with a focus on the geological section 6350 mN (A-A' in Figures 1c and 2), which represents the host volcanic succession of the H ore lens. The H ore lens represents the Chatree deposit because it is a significant ore lens with high-grade gold and massive veins containing several sulfide minerals. A detailed re-logging of old diamond drilled cores was performed in the RD5144, RD1121, RD1120, RD397, RD453, RD394, RD384, RD374, RD449, RD344, and RD 477 holes located from NW to SE along the A-A' section (Figure 2). Attention was paid before the sampling to collect ore and host rock samples systematically from the footwall and hanging wall zones. Subsequently, ore and host rock samples were collected from different host rock units. In addition, an unaltered lithic-rich fiamme breccia sample was collected from away from the ore zone, at approximately 300 m north of the ore zone of the H ore lens, to represent a background sample (Figure 1c).
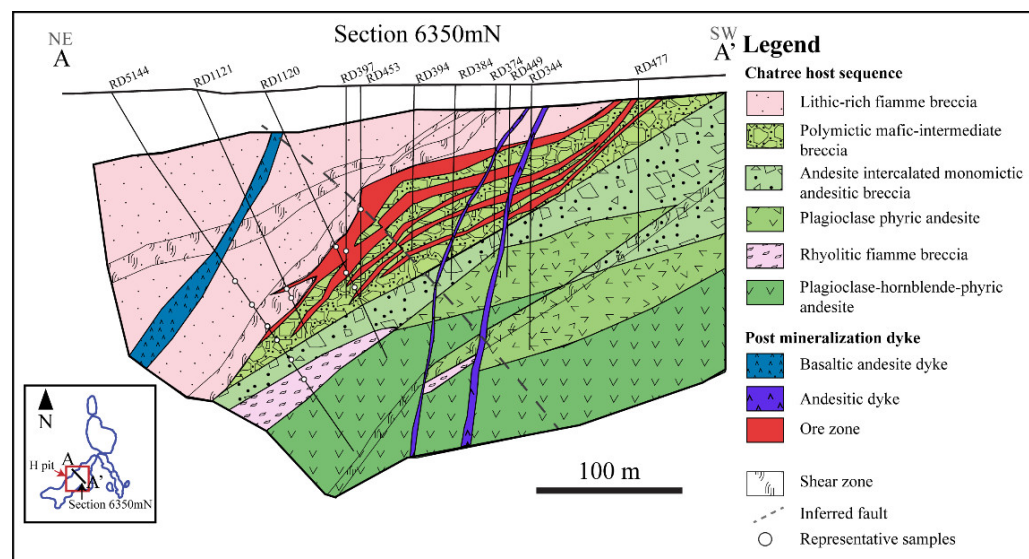
Figure 2. The representative geological cross section of the H-pit along A-A' (section no. 6530 mN) showing all rock types of the host sequence and ore zone. Note that the ore zone and rocks of the host rock sequence are often cross-cut by post-mineralization basaltic andesite and andesite dykes. Data modified after [30].

As a result, 30 host rock and vein (or ore) samples were collected. They were investigated using a microscope under reflected and polarized light to determine rock types and sulfide minerals, including estimating the abundance of sulfide minerals (particularly

pyrite). Sulfide mineral percentages were visually estimated with the naked eye from drill core samples (host rock and vein samples), and they are reported by using the ranges of 1 to 3%, 3 to 5%, 5 to 7%, 7 to 10%, and >10% (Table 1). ImageJ application was also applied to the hanging wall samples to confirm the percentage of sulfide minerals. The samples contain a varied amount of fine-grained disseminated pyrite, and it is hard to estimate the abundance of sulfide with the naked eye. However, the application can provide a precise number for evaluating such sulfide minerals [37].

All types of sulfide minerals identified under a microscope were confirmed by their chemical compositions using EPMA, with particular preference given to fine-grained unidentified sulfide minerals. In addition, a sulfide investigation was conducted to measure their trace element chemistry. An electron probe micro-analyzer (EPMA), JEOL model JXA 8100, was used to investigate the chemical composition of minerals, particularly sulfide minerals (e.g., As, Cd, Co, Cr, Cu, Mn, Ni, Pb, Zn, Fe, S) at the Department of Geology, Chulalongkorn University, Thailand. The operating conditions of EPMA included an accelerating voltage of 15 kV, a beam current of 25 nA, and an electron beam diameter of 1 μm. The microprobe standards are as follows: pure metal standards (e.g., Cd, Cr, Cu, Ni, Pb, and Fe), oxide standards (e.g., Co, Mn, and Zn), and mineral standards (e.g., As, Fe, and S). The details of the X-ray characteristics are listed in the Supplementary Materials (Table S1). Finally, fourteen representative samples (Table 1) were selected for chemical analysis using EPMA to investigate aspects of ARD and heavy metal contents.

Table 1. Summary description and mineral content of the samples from the H ore lens of the Chatree deposit.

Sample Location	Sample No.[1]	Sample Types	Description	Estimation of Sulfide Content (%)	
				Visual Estimation	ImageJ
Ore zone	397-124.6	Vein	Quartz-carbonate-chlorite-sulfide vein	1–3	-
	397-132	Vein	Quartz-carbonate-chlorite-sulfide vein	1–3	-
	453-85.3	Vein	Quartz-carbonate-chlorite-sulfide vein	3–5	-
	1120-136.7	Vein	Massive pyrite-quartz vein	3–5	-
	1121-164.5	Vein	Quartz-carbonate-chlorite-sulfide vein with sulfides along vein selvages	3–5	-
Hanging wall	1121-168	Lithic-rich fiamme breccia	Pyrite dissemination selectively in volcanic clasts	7–10	5–>10
	5144-179.6	Lithic-rich fiamme breccia	Abundant disseminated pyrite	7–10	5–>10
	5144-190.4	Lithic-rich fiamme breccia	Moderate amount of disseminated pyrite	7–10	5–7
	5144-195	Lithic-rich fiamme breccia	Moderate amount of disseminated pyrite	7–10	5–7
Footwall	1120-157.3	Polymictic mafic to intermediate breccia	Breccias consisting of mixed sedimentary and volcanic clasts	3–5	-
	5144-215	Polymictic mafic to intermediate breccia	Presence of some veinlets containing sulfides	5–7	-
	5144-237	Plagioclase phyric andesite	Unaltered	1–3	-
	5144-244.1	Rhyolitic fiamme breccia	Unaltered	1–3	-
Background	Unmineralized	Lithic-rich fiamme breccia	Similar rock unit in the hanging wall zone, collected at the unmineralized	1–3	-

| | area approximately 300 m away from the ore zone of the H ore lens |

[1] X-Y; X = drill hole number, Y = depth (meter).

3.2. Acid Rock Drainage (ARD) Assessment

The term ARD was used in this study to emphasize the acid-forming potential of the vein and host rock samples collected from the H ore lens drilled cores at the Chatree deposit. The study used static tests to evaluate the acid-forming potential (AFP) for ARD classification [4,38]. The static test of acid-base accounting (ABA) was assessed by determining the maximum potential acidity (MPA), acid neutralizing capacity (ANC), net acid-producing potential (NAPP), net acid generation (NAG), paste pH, and acid potential ratio (APR) [14,39]. The MPA was investigated from the total sulfur contents, which were detected using a LECO 628 series (CHNS determinator) at the Scientific and Technological Research Equipment Center (STREC), Chulalongkorn University, Thailand, and the MPA values were obtained from the sulfur contents multiplied by 30.6 [5,40]. The ANC was determined by adding excess acid and then back-titration with NaOH to pH 7 to determine the amount of residual acid, which can be represented by carbonate content [41]. NAPP was calculated by the difference between MPA and ANC. In addition, the NAG test was performed by determining the oxidation of samples containing sulfide minerals with H_2O_2 [5]. Then, the final pH of the NAG test (NAGpH) was measured using a pH meter. The paste pH of samples was collected by pH of the sample in deionized water for 12–16 h at a solid/water ratio of 1:2 (*w/w*) [4]. The ratio of ANC to MPA calculated the APR, and the acid-forming potential can be evaluated using the APR values by following the criteria of Lei and Watkins [39]. Furthermore, the plots between NAPP and NAGpH were used to classify the ARD potential using the classification scheme of Smart et al. [4]. The paste pH and NAGpH values were also plotted using the classification fields of Price [11,42], which can indicate AFP with lagtime to acid formation.

3.3. Total Heavy Metal Analysis

The total digestion method was used to analyze the heavy metal concentrations in the samples. First, powdered samples were digested using EPA 3052 acid digestion to investigate the total content of heavy metals (i.e., As, Cr, Cd, Cu, Ni, Mn, Pb, Zn). Next, 0.5 g sample powder was added into the vessel in a fume hood and digested with 3 mL concentrated HF and 9 mL concentrated HNO_3. The samples were heated to 180 ± 5 °C for approximately 5.5 min and remained for 9.5 min. After microwave digestion, they were evaporated two times to eliminate the remaining HF. Final substances were made in volume by 100 mL of 1% HNO_3. Finally, the samples were analyzed by an Inductively coupled plasma-optical emission spectrometer (ICP-OES) at the Department of Mineral Resources, Thailand. In addition, the rock standards from USGS (AGV-2 and BHVO-2) and GSJ (JB-1b and JG-2) are used in this analysis as well. The contents of the heavy metals in the samples were obtained. The detection limits for each element are as follows: 0.1 mg/kg of As, 0.5 mg/kg of Cr, 0.15 mg/kg of Cd, 0.1 mg/kg of Cu, 2 mg/kg of Ni, 15 mg/kg of Mn, 2 mg/kg of Pb, and 0.1 mg/kg of Zn.

4. Results

4.1. Geology of the H-Pit

The main geological cross section (section A-A') of the H-pit (ore lens) is given in Figure 2. The rocks in the host sequence can be distinctly classified into hanging wall and footwall zones regarding vertical positions against the ore zone, which is predominantly hosted in a polymictic mafic-intermediate breccia unit (Figure 2). The footwall zone comprises mainly coherent andesite with minor breccia units, whereas the hanging wall zone consists only of the lithic-rich fiamme breccia unit. Post-mineralization dykes ranging in composition from basaltic andesite to andesite commonly occur at the H ore lens. They

cross-cut all earlier units, including mineralized veins in the ore zone. Detailed petro-graphic descriptions of the ore and host rock units are made below in ascending order from the bottom to the top of the succession (Figure 3).
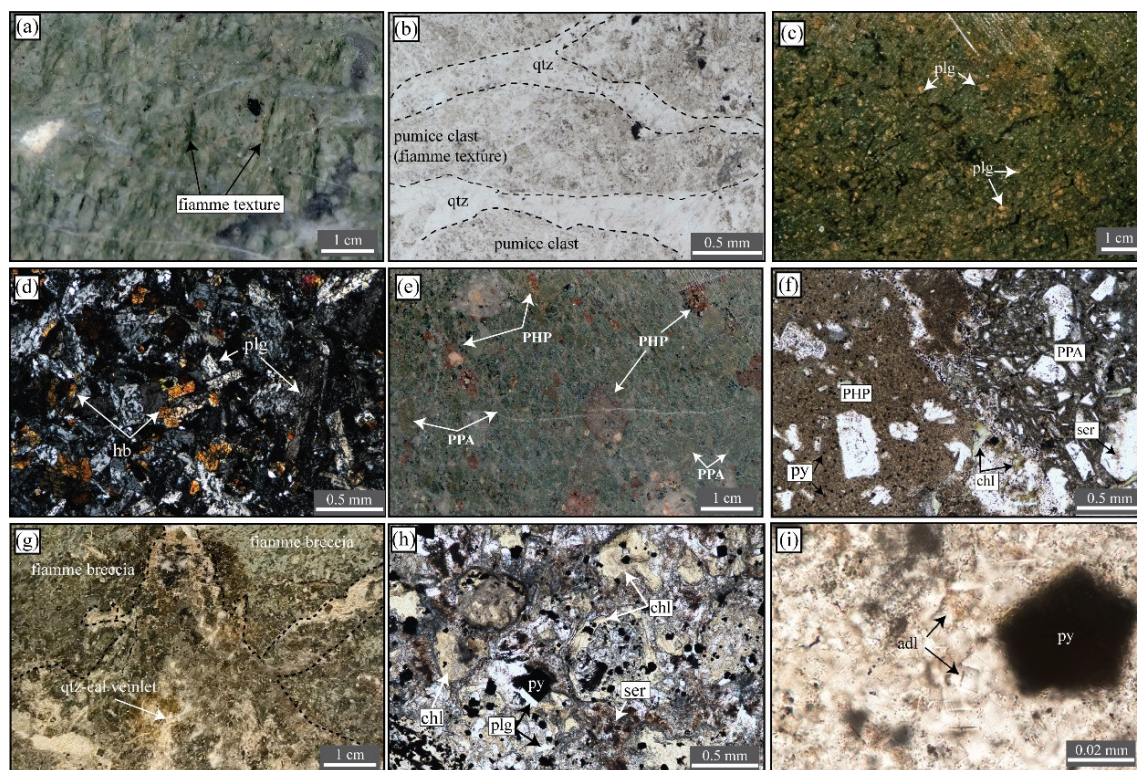

Figure 3. Photograph and photomicrograph of representative host rock samples. (**a**) Photograph of rhyolitic fiamme breccia showing a flame-like texture (fiamme). (**b**) Photomicrograph of rhyolitic fiamme breccia showing quartz crystals and pumice clasts (PPL). (**c**) Photograph of plagioclase phyric andesite. (**d**) Photomicrograph of plagioclase phyric andesite showing plagioclase and pyroxene phenocrysts (XPL). (**e**) Photograph of polymictic mafic-intermediate breccia showing clasts of plagioclase-hornblende phyric andesite and plagioclase phyric andesite. (**f**) Photomicrograph of polymictic mafic-intermediate breccia showing clasts in several types, such as plagioclase-hornblende phyric andesite, plagioclase phyric andesite, and sandstone (PPL). (**g**) Photograph of lithic-rich fiamme breccia showing intense alteration in the rock. (**h**) Photomicrograph of lithic-rich fiamme breccia showing an abundance of alteration minerals, such as sericite, chlorite, and pyrite. (**i**) Photomicrograph of lithic-rich fiamme breccia showing adularia and pyrite as alteration minerals that occurred close to the veins. Abbreviations: chl = chlorite, py = pyrite, plg = plagioclase, hb = hornblende, qtz = quartz, ser = sericite PHP = plagioclase-hornblende phyric andesite, PPA = plagioclase phyric andesite, adl = adularia.

(1) The footwall zone consists of plagioclase-hornblende-phyric andesite at the bottom and the overlying unit of the plagioclase phyric andesite, with thin intercalating layers of rhyolitic fiamme breccia.

The plagioclase-hornblende-phyric andesite is a coherent unit. It has a porphyritic texture in which phenocrysts are mainly plagioclase and hornblende, with a fine-grained plagioclase-hornblende groundmass. The plagioclase and hornblende phenocrysts range from 0.1 to 1 cm and 0.05 to 0.2 cm in size, respectively.

The rhyolitic fiamme breccia occurs only in the western part of the H ore lens. This breccia unit is composed mainly of pumice clasts and quartz crystals ranging from 2 mm to 3 cm in size (Figure 3a,b). The pumice clasts commonly show an elongated "fiamme" texture, and most of the fiamme clasts are altered to chlorite. This rock contains 1%–3% of pyrites by visual estimation in the field, as shown in Table 1.

The plagioclase phyric andesite occupies the eastern part of the H ore lens. It is approximately 50 m thick. The unit shows a grayish-green color with spots of orange

plagioclase (iron-stained plagioclase) in the drilled cores (Figure 3c). Under the microscope, it mainly consists of interlocking laths of plagioclase and hornblende crystals (Figure 3d), and the plagioclase crystals are generally altered by sericite, and calcite. This unit is overlain by andesite intercalated monomictic andesitic breccia, which is characterized by monomictic andesitic breccia, partly interbedded with coherent andesite layers/lenses. The monomictic andesitic breccia commonly displays a jigsaw-fit texture of plagioclase phyric andesite clasts with a matrix of andesite compositions. Pyrites have low contents ranging from 1%–3% (Table 1).

(2) The unit in the ore zone comprises only a polymictic mafic-intermediate breccia unit (Figure 3e), which is stratigraphically distinct from the above hanging wall. It overlies the andesite intercalated monomictic andesitic breccia with gradational contact. The polymictic mafic-intermediate breccia consists mainly of subangular to angular clasts of plagioclase-hornblende-phyric andesite, plagioclase phyric andesite, sandstone, and mudstone (Figure 3e,f). The unit shows a matrix-supported texture with the andesite clasts ranging from 2 to 8 mm in size in the upper part of the unit and clast-supported texture in the lower part involving 1–2 cm size clasts. The matrix is an andesite composition. Sericite, chlorite, and pyrite are also found as alteration minerals in this rock. This rock contains 3%–7% pyrites (Table 1).

(3) The hanging wall zone is composed of the fiamme breccia unit, which is predominant in lithic-rich fiamme breccia, with minor crystal-rich fiamme breccia. This unit overlies the polymictic mafic-intermediate breccia unit hosting the ore zone with sharp contact. The lithic-rich fiamme breccia is made up of fiamme/pumice clasts and minor rock fragments (Figure 3g). The fiamme contains some quartz crystals ranging from 1 to 2 mm. The rocks strongly altered and became richer in the sericite-pyrite-chlorite-quartz-adularia assemblage (Figure 3h,i). Quartz and adularia are found in a silica-rich zone close to veins, whereas sericite and chlorite are abundant in rocks far from veins. Pyrite is commonly found in the whole unit as disseminated pyrite and is abundantly present in the shear zone at the deeper part of the unit or in proximity to the mineralized veins/ore zone. The disseminated pyrites generally have subhedral to euhedral crystals with a size of 10–200 µm (Figure 3h). The estimation of sulfide minerals in the hanging wall is presented in Table 1. The hanging wall zone contains 7%–10% by visual estimation and 5%–>10% by ImageJ.

4.2. Mineralization

The ore zone of the H ore lens occurs as a narrow zone at the surface, sprays into several layers at the middle part, forming a wide ore zone, and again becomes a narrow zone and pinches out at the deeper part (Figure 2). The ore zone is represented by Au-Ag mineralization, which occurs mainly as veins/veinlets with minor breccia. They are predominantly hosted in the polymictic mafic-intermediate breccia unit. Based on cross-cutting and overprinting relationships, mineral assemblages, and textural features of veins/veinlets and breccias, at least four mineralization stages are identified at the H ore lens with a main Au-Ag bearing event at stage 3 (Figure 4).

Stage 1 (quartz ± pyrite vein) is characterized by light to dark gray microcrystalline quartz with rare pyrite (Figure 5a). It commonly occurs as vein, stockwork, and minor breccia. Pyrite is rare, but where present, it appears as fine-grained pyrite aggregates situated along the edges of veins as a black band. Stage 2 forms a pyrite-rich quartz vein (Figure 5b) and is characterized by light gray quartz, with abundant pyrite presenting as patches in the vein. Sulfide minerals in stage 2 consist mainly of pyrite-forming aggregates of subhedral to euhedral crystals (Figure 5c). No gold has been identified at this stage. Stage 3 is the main Au-Ag mineralization stage of the H ore lens and is represented by a quartz-carbonate-chlorite-sulfide-electrum vein (Figure 5d). It is characterized by colloform vein textures. The veins at this stage consist of white to pale gray quartz with chlorite and sulfide-rich bands (Figure 5d). Sulfides at this stage comprise assemblages of pyrite and minor sphalerite, chalcopyrite, and galena (Figure 5e). Pyrite is subhedral to euhedral

in shape and associates intimately with other sulfides (e.g., sphalerite, galena, chalcopyrite). Chalcopyrite tends to form as a very fine-grained dissemination in sphalerite crystals (i.e., chalcopyrite disease texture). The pyrite in the vein commonly has a larger size than pyrite in host rock (up to 300 μm; Figure 5e). Gold occurs as an electrum and generally forms free grains associated with quartz, calcite, and sulfide minerals. The electrum is also quite common to form as inclusions of sulfides, especially pyrite. It was observed that a high concentration of disseminated pyrite is present in the wall rock of the hanging wall zone in proximity to the stage 3 veins (Figure 5d; up to a few tens cm from veins). Stage 4 occurs as quartz-carbonate veins/veinlets and is characterized by white quartz on the edge of the veins or envelopes of breccia fragments in the veins, while white to pinkish-white carbonate occurs in the inner part of the veins (Figure 5f). The stage 4 veins contain no gold or sulfide minerals and are widely distributed across the H ore lens area and cross-cut veins of all earlier stages.
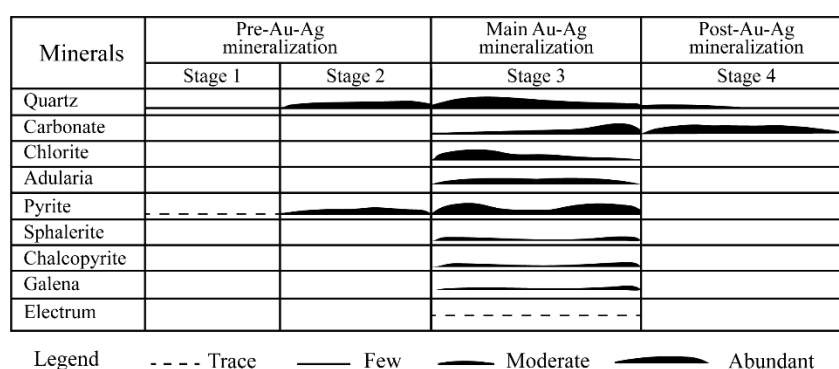
Minerals	Pre-Au-Ag mineralization		Main Au-Ag mineralization	Post-Au-Ag mineralization
	Stage 1	Stage 2	Stage 3	Stage 4
Quartz				
Carbonate				
Chlorite				
Adularia				
Pyrite				
Sphalerite				
Chalcopyrite				
Galena				
Electrum				

| Legend | - - - - Trace | —— Few | Moderate | Abundant |

Figure 4. Paragenesis diagram of mineralization at the H ore lens showing the occurrences and relative abundance of minerals in each mineralization stage.
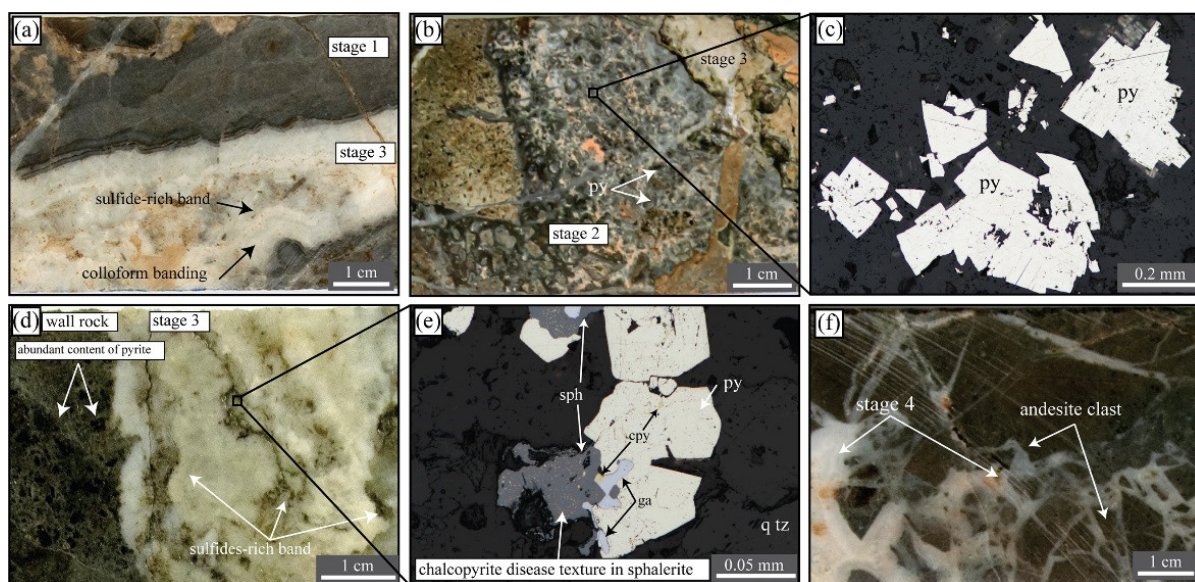

Figure 5. Characteristics of veins and mineral assemblages at each mineralization stage of the H ore lens in the Chatree deposit. (**a**) Photograph of the stage 1 vein showing the gray quartz vein cut by the stage 3 vein. Sample No. 397-144.6. (**b**) Photograph of the stage 2 vein showing a massive pyrite-quartz vein. Sample No. 1120-136.7. (**c**) Photomicrograph of pyrite located in the stage 2 vein showing euhedral texture. (**d**) Photograph of quartz-carbonate-chlorite-sulfide-electrum vein of stage 3 showing dark sulfide-rich bands in the white quartz-chlorite band. Sample No. 5144-214. (**e**) Photomicrograph of sulfides in the stage 3 vein consisting of pyrite, sphalerite, chalcopyrite, and galena. (**f**) Photograph of quartz-carbonate vein of stage 4 hosted in andesite showing barren quartz-carbonate vein. Sample No. 1120-130.3. Abbreviations: py = pyrite, cpy = chalcopyrite, sph = sphalerite, ga = galena, qtz = quartz.

4.3. Geochemistry of Sulfide Minerals

The results of the EPMA spot analysis are summarized in Table 2, and the full results are listed in SupplementaryMaterials (Tables S2–S4). The samples were collected from stage 3 quartz-carbonate-chlorite-sulfide-electrum veins and from one sample containing high sulfides (pyrite) in the hanging wall zone. In addition, EPMA elemental mapping was conducted on the selected vein sample in stage 3 (see Figure 6). This mapping shows the distribution of some trace elements. This demonstrates that arsenic (As), which could be incorporated into any sulfide in this sample, is selectively and preferentially present in galena and pyrite (Figure 6).

Table 2. Summary results of EPMA spot analysis (wt.%) of galena, sphalerite, chalcopyrite, and pyrite in quartz-carbonate-chlorite-sulfide-electrum veins (stage 3) and pyrite in the hanging wall zone.

Minerals			As	Cd	Co	Cr	Cu	Mn	Ni	Pb	Zn	Fe	S
Galena (n = 18)	Max		0.98	<0.07	0.02	0.05	1.54	0.09	0.04	88.03	0.69	1.52	12.81
	Min		<0.04	<0.07	<0.02	<0.02	<0.03	<0.02	<0.02	85.79	<0.05	<0.02	10.00
	Avg		0.23	-	<0.02	<0.02	0.13	0.02	<0.02	86.75	<0.05	0.52	11.85
	SD		0.38	-	<0.02	<0.02	0.37	0.03	<0.02	0.60	0.16	0.41	0.85
Sphalerite (n = 15)	Max		<0.04	0.18	<0.02	0.04	1.99	0.07	0.02	0.09	62.88	3.85	33.92
	Min		<0.04	<0.07	<0.02	<0.02	0.05	<0.02	<0.02	<0.05	61.41	1.53	32.31
	Avg		-	0.06	-	<0.02	1.16	0.02	<0.02	<0.05	61.99	2.61	33.35
	SD		-	0.07	-	<0.02	0.54	0.03	<0.02	<0.05	0.41	0.68	0.43
Chalcopyrite (n = 9)	Max		<0.04	<0.07	<0.02	<0.02	33.87	<0.02	<0.02	0.09	0.23	32.92	32.49
	Min		<0.04	<0.07	<0.02	<0.02	33.14	<0.02	<0.02	<0.05	<0.05	32.12	31.91
	Avg		-	-	-	-	-	-	-	<0.05	0.06	32.64	32.31
	SD		-	-	-	-	-	-	-	-	0.08	0.23	0.21
Pyrite in vein (n = 76)	Max		0.94	<0.07	<0.02	0.05	0.74	0.06	<0.04	<0.05	0.11	46.74	53.99
	Min		<0.04	<0.07	<0.02	<0.02	<0.03	<0.02	<0.04	<0.05	<0.05	40.20	52.02
	Avg		0.20	-	-	<0.02	0.05	<0.02	-	-	<0.05	45.29	53.00
	SD		0.24	-	-	<0.02	0.13	0.02	-	-	<0.05	1.23	0.51
Pyrite in the hangingwall (n = 47)	Max		0.07	<0.07	<0.02	0.03	0.26	0.06	<0.04	<0.05	0.07	49.74	53.27
	Min		<0.04	<0.07	<0.02	<0.02	<0.03	<0.02	<0.04	<0.05	<0.05	45.87	49.73
	Avg		<0.04	-	-	<0.02	0.03	<0.02	-	-	<0.05	47.56	51.37
	SD		<0.04	-	-	<0.02	0.04	0.02	-	-	<0.05	0.83	0.76

As a result, it was found that As and Cd are distinctly concentrated in specific sulfide minerals. A high concentration of As is illustrated in galena and pyrite in veins yielding 0.23 avg. wt.% and 0.20 avg. wt.%, respectively (Table 2). The content of Cd (avg. 0.06 wt.%) is involved in sphalerite. Moreover, it can be noted that an amount (avg. 1.16 wt.%) of Cu is also present in sphalerite, probably due to the presence of chalcopyrite disease. A comparison of the data between the pyrites in the vein and the hanging wall indicates that As content is distinctively elevated in the vein pyrite (avg. 0.94 wt.%), showing that it is approximately 20 times greater than the hanging wall pyrite at maximum values (max 0.07 and avg. <0.04). However, some trace elements, including Co, Cr, and Ni, are lower than the detection limit in average values. Furthermore, carbonate in veins was defined as calcite with an average stoichiometric formula as $Ca_{0.987}Mg_{0.005}Fe_{0.000}Mn_{0.017}CO_3$. The Mn content in calcite is 0.86–1.35 wt.%. EPMA data are presented in Supplementary Table S5.
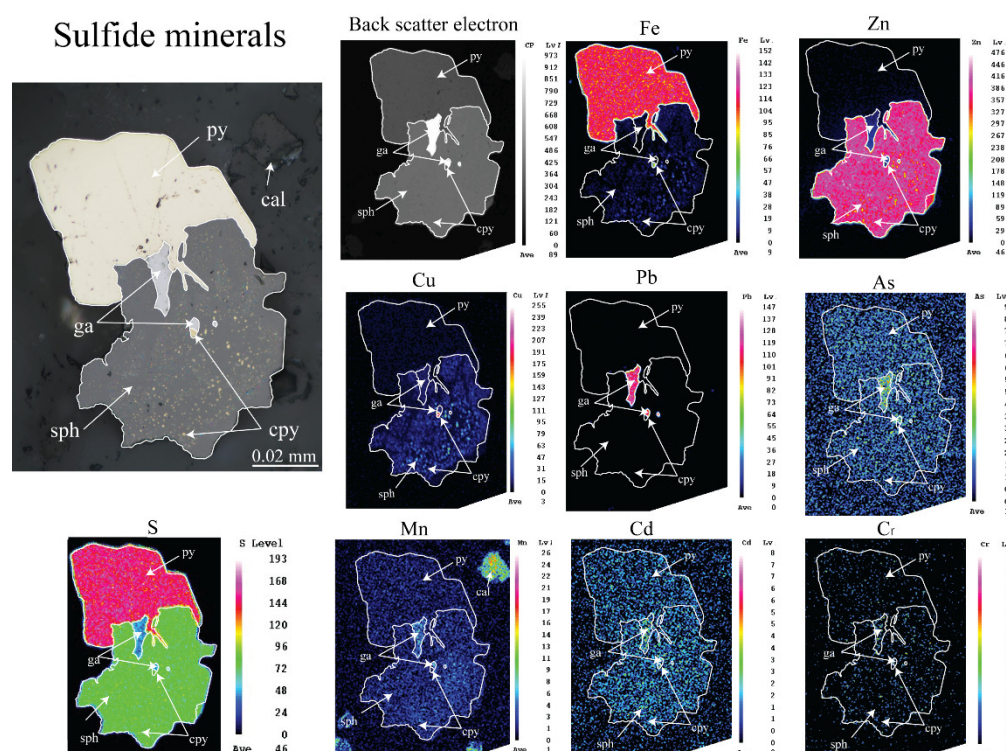
Figure 6. Photomicrograph, back scatter electron, and EPMA elemental map images of aggregated sulfide minerals in the quartz-carbonate-chlorite-sulfide-electrum vein (stage 3). Abbreviations: py = pyrite, cal = calcite, sph = sphalerite, cpy = chalcopyrite, ga = galena.

4.4. Acid Rock Drainage (ARD) Assessment

The fourteen samples listed in Table 1 were investigated for the static acid-base accounting (ABA) and net acid generation (NAG) tests to assess ARD potential. The results are presented in Table 3.

The ARD classification results of the tested samples using schemes by Lei and Watkins [39], Smart et al. [4], and Price [42] are listed in Table 3.

The results by a scheme of Lei and Watkins [39] show that all of the ore zone, footwall zone, and background samples are classified as non-acid forming (NAF) materials except samples 5144-215 and 1121-164.5, which are classified as uncertain (UC) materials. On the other hand, most hanging wall samples are identified as potential acid-forming (PAF) materials, with one sample (sample 5144-195) indicated as UC material.

The ARD classification results using the scheme of Smart et al. [4] are visually displayed in Figure 7a, revealing that all of the ore zone, footwall zone, and background samples are classified as NAF materials, except for sample 5144-215, which is identified as UC material. In contrast, all hanging wall zone samples are classified as PAF materials except for one sample (sample 5144-195) classified as UC material.

Nevertheless, the ARD classification results using the discrimination scheme of Price [42] are given in Figure 7b. The results indicate that all the background, ore zone, and footwall zone samples are NAF materials. On the other hand, almost all hanging wall zone samples are classified as PAF with a rapid ARD-medium risk category. Still, one hanging wall zone sample (sample 5144-195) is classified as NAF material.

Table 3. Summary of the ABA and NAG test results of the representative samples from the H ore lens of the Chatree deposit.

| Sample Location	Sample No.	Sample Types	% Sulfur	MPA (kg H₂SO₄/t)	ANC (kg H₂SO₄/t)	NAG (kg H₂SO₄/t)	NAG pH	NAPP (kg H₂SO₄/t)	Paste pH	APR	Classification		
											Lei and Watkins [39]	Smart [4]	Price [42]
Ore zone	397-124.6	Vein	0.10	3.06	162.52	0.00	7.44	−159.46	6.21	53.11	NAF	NAF	NAF
	397-132	Vein	0.18	5.51	233.12	0.00	7.63	−227.62	6.30	42.33	NAF	NAF	NAF
	453-85.3	Vein	0.30	9.18	241.70	0.00	7.81	−232.52	6.78	26.33	NAF	NAF	NAF
	1120-136.7	Vein	1.88	57.53	209.09	3.92	5.44	−151.56	6.68	3.64	NAF	NAF	NAF
	1121-164.5	Vein	1.91	58.45	142.72	0.00	7.76	−84.28	6.02	2.44	UC	NAF	NAF
Hanging wall	1121-168	Lithic-rich fiamme breccia	3.10	94.86	73.39	19.55	3.91	21.47	5.81	0.77	PAF	PAF	PAF
	5144-179.6	Lithic-rich fiamme breccia	3.22	98.53	68.57	47.98	2.13	29.96	5.45	0.70	PAF	PAF	PAF
	5144-190.4	Lithic-rich fiamme breccia	2.25	68.85	47.02	37.11	2.20	21.83	5.60	0.68	PAF	PAF	PAF
	5144-195	Lithic-rich fiamme breccia	2.44	74.66	63.48	1.96	4.67	11.18	6.10	0.85	UC	UC	NAF
Footwall	1120-157.3	Polymictic mafic to intermediate breccia	0.30	9.18	108.29	0.00	7.49	−99.11	6.63	11.80	NAF	NAF	NAF
	5144-215	Polymictic mafic to intermediate breccia	2.88	88.13	74.44	1.96	4.80	13.69	6.12	0.86	UC	UC	NAF
	5144-237	Plagioclase phyric andesite	0.19	5.81	120.24	0.00	7.73	−114.43	6.30	20.68	NAF	NAF	NAF
	5144-244.1	Rhyolitic fiamme breccia	0.12	3.67	100.89	0.00	7.70	−97.22	6.28	27.48	NAF	NAF	NAF
Background	Unmineralized	Lithic-rich fiamme breccia	0.05	1.53	57.73	9.77	5.19	−56.20	6.19	37.73	NAF	NAF	NAF
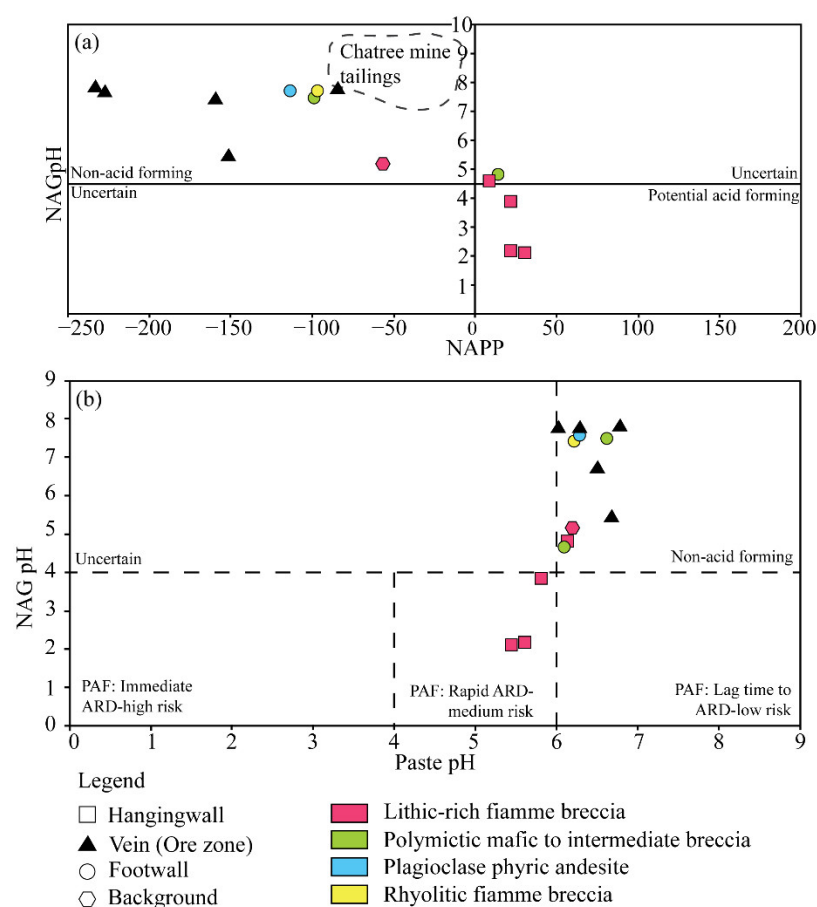
Figure 7. Classification of the ARD potential of the representative ore and host rock samples from the H ore lens of the Chatree deposit. (**a**) Plots using the classification scheme of Smart et al. [4] showing all of the lithic-rich fiamme breccia samples plot on the PAF field or on a boundary with UC field, whereas plots of all the rest samples are on NAF field except one footwall sample plotted on UC field. The data field of Chatree mine tailings is from Changul et al. [13]. (**b**) Plots using the classification scheme of Price [42] showing three of four hanging wall lithic-rich fiamme breccia samples plotted on the PAF's rapid ARD-medium risk field. In contrast, all the remaining samples are placed on the NAF field.

4.5. Total Trace Metals and Metalloids

The results of trace metals and metalloids in the fourteen tested samples from the ore, hanging wall, and footwall zones of the H ore lens with a background sample are summarized in Table 4, along with the reported values of typical igneous rocks.

Table 4. Trace metal and metalloid concentrations (mg/kg) in the representative samples from the H ore lens, with values of typical igneous rocks.

Sample Location	Sample No.	Sample Types	As	Cd	Cr	Cu	Mn	Ni	Pb	Zn
	397-124.6	Vein	23.4	6.20	16.1	131	607	13.3	9.83	112
	397-132	Vein	73.6	9.59	24.4	130	596	10.0	16.1	161
Ore zone	453-85.3	Vein	75.4	2.05	34.2	49.6	1523	29.7	21.6	130
	1120-136.7	Vein	22.7	1.82	8.42	26.4	1686	23.2	34.2	195
	1121-164.5	Vein	19.8	4.34	14.20	79.0	1609	27.2	40.3	142
	1121-168	Lithic-rich fiamme breccia	2.50	1.21	15.9	25.2	1673	14.3	19.2	80.3
Hanging wall	5144-179.6	Lithic-rich fiamme breccia	3.57	2.12	12.7	26.9	1482	12.9	11.2	116
	5144-190.4	Lithic-rich fiamme breccia	2.16	2.20	24.3	29.2	1357	7.74	24.7	128
	5144-195	Lithic-rich fiamme breccia	7.19	4.05	18.4	32.2	730	7.07	17.2	154

Footwall	1120-157.3	Polymictic mafic to intermediate breccia	5.29	3.77	11.0	29.4	675	6.12	12.1	113
	5144-215	Polymictic mafic to intermediate breccia	3.11	0.30	17.30	27.5	837	16.2	14.2	148
	5144-237	Plagioclase phyric andesite	<0.10	0.83	28.1	28.3	593	24.3	13.1	114
	5144-244.1	Rhyolitic fiamme breccia	<0.10	0.12	20.3	26.9	627	6.37	4.23	59.3
Background	Unmineralized	Lithic-rich fiamme breccia	<0.10	0.96	18.1	4.3	461	7.50	18.6	78.3
	Typical igneous rock	Granite [1]	2	0.13	10	20	450	10	17	50
		Andesite [2]	2	0.17	56	54	1200	18	6.7	70
		Basalt [1]	2.2	0.21	185	94	1800	145	7	118

[1] Granite and basalt [43,44], [2] Andesite [45,46].

5. Discussion

Several published papers assess the environmental aspects of the Chatree mine [8,13,14,16,17,47], and these studies discuss and conclude a wide range of potential environmental issues at the Chatree, including potential AMD generation in the future. However, the data produced in previous studies are based principally on samples collected either from the waste dump or tailing sites where mixed materials are stored. Little/no information about the original rocks is preserved, so the source materials that generate the suggested potential risks were not well identified (e.g., a source was not identified for the high Mn content in tailing). Therefore, the discussions made here are intended to include such information to identify the sources of the potential environmental risks recognized in the H ore lens results.

5.1. Geology and Mineralization Styles of the H ore Lens

The results of this study revealed that the ore zone at the H ore lens comprises mainly veins/veinlets with minor breccias, and the ore zone forms under strong lithological control. Consequently, the ore zone of the H-pit is hosted predominantly in the polymictic mafic-intermediate breccia unit. The footwall zone is mostly composed of coherent volcanic rocks, such as plagioclase-hornblende-phyric andesite and plagioclase phyric andesite. The hanging wall with the ore zones, on the other hand, is dominated by uncoherent volcanic rocks, including the lithic-rich fiamme breccia unit (Figure 2). As a result, the composition of the volcanic host rock succession changes from coherent to incoherent volcanic units around the ore zone. This transitional zone is recognized as a preferred gold depositional window in the Chatree district due to the presence of major ore lenses in the zone, and it is regarded as the best exploration target.

Based on the textural characteristics of the mineralized and unmineralized veins, with their cross-cutting and overprinting relationships, four mineralization stages are established in this study. The main Au-Ag mineralization occurs in stage 3, as quartz-carbonate-chlorite-sulfide-electrum veins (Figure 4), with distinguished open space-filing vein textures (e.g., colloform bandings; Figure 5). The sulfide minerals of stage 3 involve major pyrite and minor chalcopyrite, sphalerite, and galena. The occurrence of the sulfide mineral assemblage is confined to mineralized veins. However, disseminated pyrites are also present in the hanging wall zone in proximity to the ore zone. The disseminated pyrites are formed as alteration minerals. The alteration minerals in the hanging wall, including sericite-chlorite-pyrite-adularia (Figure 3g–i), found in the hanging wall rocks, can be considered as argillic alteration, which is equivalent to the illite-quartz-adularia-chlorite-calcite-pyrite alteration zone of Salam [29]. Adularia is an indicator of boiling in the LS epithermal environment because it is the result of alkaline fluids produced from boiling [48]. The mole percent of FeS in sphalerite coexisting with pyrite can be used to define the sulfidation state [49]: low sulfidation state (40–20 mole% FeS), intermediate sulfidation state (20–1 mole% FeS), high sulfidation state (1.0–0.05 mole% FeS), and very high

sulfidation state (<0.05). The FeS mole percent in sphalerite in this deposit range is 2.69–6.65 mole% (Supplementary material Table S6), which can be defined as an intermediate sulfidation state. However, some studies have reported that LS deposits can contain <20 mole% FeS, such as LS deposits, in the National and Temascaltepec districts [6,50,51].

However, other geological characteristics, including textural features of quartz, alteration, and mineral assemblages, allow us to classify the H ore lens into a low-sulfidation epithermal deposit model, similar to other ore lenses presented in the Chatree deposit [28,30,31,33]. Furthermore, the H ore lens is considered to represent the deeper part of the epithermal system, as higher contents of base metal sulfides (i.e., chalcopyrite, galena, sphalerite) are found in the H ore lens compared to other lenses at the Chatree deposit [30].

5.2. Acid Rock Drainage Potential

The high content of sulfides in the lithic-rich fiamme breccias as disseminated pyrites may cause this PAF classification. It is characterized by low NAGpH values, which are principally contributed by the sulfur content in the samples. High sulfur content is typically linked to acid-forming potential [3,52,53]. However, it is noted that some vein samples also contain relatively high sulfur (i.e., Samples 1120-136.7 and 1121-164.5 contain approximately 1.9% sulfur; Table 3). Such samples are not classified as PAF materials in Figure 7, probably due to high carbonate content, as indicated by high ANC values in the samples. Since high carbonate content in samples can elevate ANC values and buffer acidic conditions [10], this is the case for such vein samples to be classified as NAF. The results of the petrographic study also confirm that carbonate minerals are commonly present in the vein samples (Figures 4 and 5).

The geological cross-section of the H ore lens and the ARD static test results are illustrated in Figure 8, which shows that the hanging wall zone is classified as PAF, whereas the ore and footwall zones are NAF. As discussed above, it is considered that the presence of abundant disseminated pyrite (5%–>10% in volume; Table 1) in the hanging wall lithic-rich fiamme breccia unit causes the discrimination of this unit into PAF rock. The disseminated pyrites in the unit are composed predominantly of euhedral pyrite with a clean texture, a typical textural characteristic of pyrite formed by hydrothermal fluid alteration [54]. It has also been reported that abundant pyrite is an alteration mineral in volcanic or volcaniclastic host rocks of epithermal Au-Ag deposits in New Zealand [55]. The pyrites in the hanging wall occur from the argillic alteration with chlorite, sericite, and adularia, which is a common alteration phase of the LS epithermal deposit [30]. Therefore, it is reasonably explained that the disseminated pyrites in the hanging wall zone at the H ore lens formed in hydrothermal alteration during the main mineralizing event. It is also noticed that the hanging wall zone consisting of lithic-rich fiamme breccia is considered a permeable rock, which can have board zones of hydrothermal alteration [6].
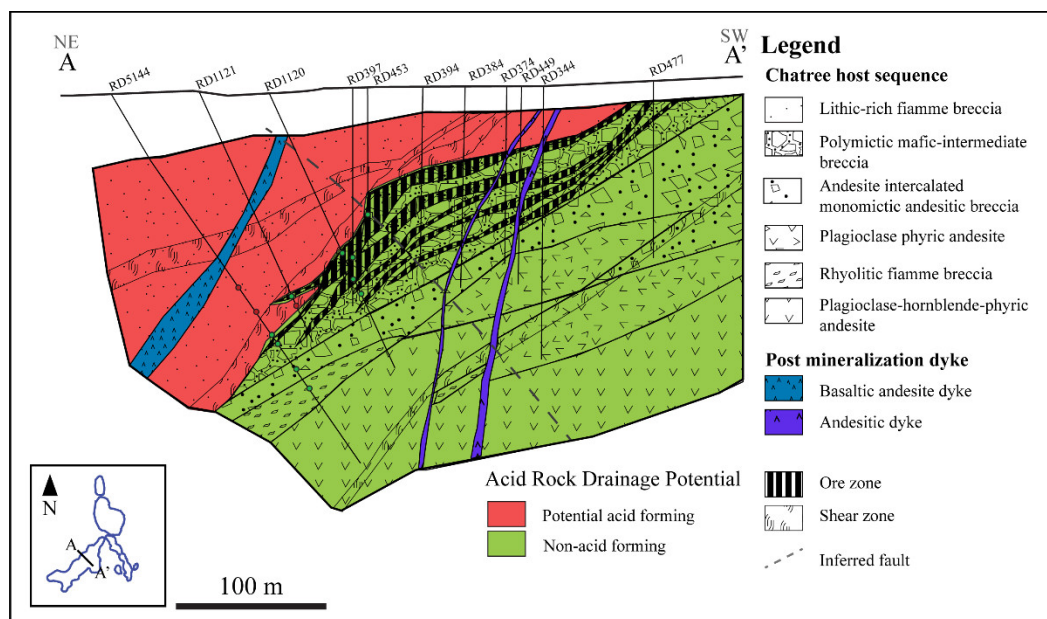
Figure 8. ARD potential classification of the ore and host rocks of the H ore lens along the A-A' cross section, indicating that the lithic-rich fiamme breccia unit in hanging wall is classified as PAF, while the ore zone and host rocks in the footwall are in the NAF classification.

The result of this study is consistent with the data in Changul et al. [14], who reported that PAF materials are identified in the silicified lapilli tuff and sheared tuff units in the C-H pit (H ore lens is a part of the C-H pit) at the Chatree mine. As the tuff units are indicated to occur in the northwestern part of the C-H pit, which corresponds to the distribution of the lithic-rich fiamme breccia unit in the hanging wall zone, the tuff units classified as PAF in Changul et al. [14] are equivalent to the PAF rocks characterized in this study. Changul et al. [13] also found that the Chatree tailing materials are classified as NAF (Figure 7a), which is compatible with this study's results, as the tailing materials are principally sourced from the mineralized veins/ore rocks that are detected to be NAF material at the H ore lens.

5.3. Trace Elements and Their Sources

The trace element contents in the samples of the ore, hanging wall and footwall zones, and background area from the H ore lens are summarized and compared using box and whisker plots (Figure 9) with typical values of igneous rocks (granite, andesite, and basalt) [43–46]. The compared data indicate that all of the tested metals (e.g., As, Cd, Cu, Mn, Pb, and Zn) are elevated in the vein samples from the ore zone compared to the hanging wall and footwall zone samples, except Cr, and Ni, which seem to be concentrated in similar mean values and value ranges. In addition, some elements, including Mn and Pb, are recognized in the hanging wall zone compared to the footwall zone. As Cu, Mn, and Zn are more enriched in the hanging wall and footwall zones at the H ore lens compared with the background sample. Cr and Ni values in the background sample are similar to the values of the hanging wall and footwall zones, whereas Pb content in the unmineralized sample is almost similar to the ore and hanging wall zones and higher than the footwall zone. The correlations of the results in this study with typical values of igneous rocks indicate that the metals and metalloids exceeding the typical igneous rock, which should be concerned in each zone are: (1) Ore zone consisting of As, Cd, Cu, Pb, and Zn; (2) Hanging wall zone comprising As, Cd, Pb, and Zn; (3) Footwall zone consisting of Cd, and Zn. However, As in the footwall only presents polymictic mafic-intermediate breccias (ore-hosted rock).
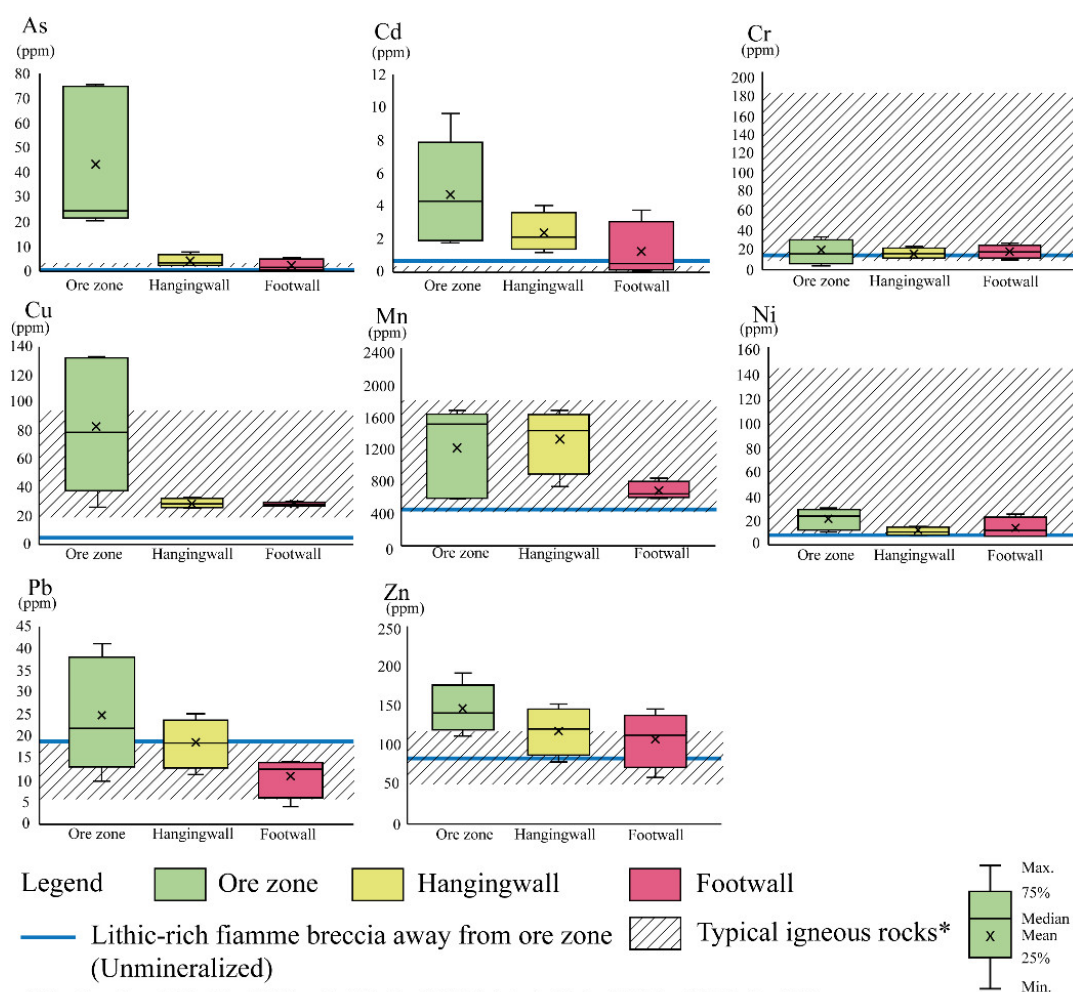
Figure 9. Box and whisker plots of heavy metal contents (e.g., As, Cd, Co, Cr, Cu, Mn, Ni, Pb, Zn) in the samples from ore (n = 5), hanging wall (n = 4), and footwall (n = 4) zones of the H ore lens at the Chatree deposit [43–46].

The heavy metals that are distinctly elevated in the ore zone (i.e., As, Cd, Cu, Pb, and Zn) compared to the hanging wall and footwall zones may be contributed from the high sulfide content in mineralized veins. The high Cu, Zn, and Pb values in the vein samples appeared to be sourced from the major components of chalcopyrite, sphalerite, and galena, respectively. In contrast, other trace elements, such as As, and Cd, are found to be present selectively in pyrite, galena, and sphalerite, as detected in the EPMA spot analysis and mapping results (Table 4; Figure 6). The elevated values of trace elements in pyrite are also reported from other ore lenses at the Chatree deposit by Salam [30], such as As. It is generally indicated that metals often substitute in pyrite as well as other sulfides in the ore zone [53,56,57], and such trace elements in pyrite tend to be incorporated into pyrite as nanoparticles [58] and within the pyrite lattice [59–61] by the hydrothermal solution during the syn-mineralization stage. George et al. [62] reported that As is rarely found as an analogous coupled substitution with Ag. Therefore, it can also be substituted for galena. This is the same as our EPMA mapping result, which illustrates that As are evenly distributed in the galena grain at the H ore lens. It is also demonstrated in the EPMA mapping result that Mn is enriched in calcite rather than in sulfide minerals in the veins (Figure 6).

5.4. Environmental Management

Our study results identify the PAF rocks in the hanging wall zone and the high concentration of some heavy metals in the ore and hanging wall zones at the H ore lens. Thus, we herein discuss potential environmental risks in these aspects at the Chatree deposit, focusing on As and Mn metals, which have previously been considered hazardous at the Chatree mine and in the surroundings.

The results of this study can provide an idea to estimate the volume of PAF rocks in the hanging wall zone. It is assumed that the spatial distribution of the lithic-rich fiamme breccia containing abundant disseminated sulfides (indicated PAF) is limited to less than a few hundred meters from the ore zone. A background sample of the lithic-rich fiamme breccia unit collected approximately 300 m from the ore zone is determined by NAF rock. It is a rough idea to draw a boundary between PAF and NAF rocks in the lithic-rich fiamme breccia unit. Further study with a closely-spaced sampling of the unit will provide data to estimate a more accurate and precise volume of PAF rocks. In addition, our test results imply that samples can be independently assessed using either of the guidelines for >0 in NAPP value, <4 in NAGpH value, or <6 in paste pH value to discriminate the PAF from NAF materials (Figure 7). This is because plots of the lithic-rich fiamme breccia of the hanging wall zone have a linear trend in Figure 7a,b. Thus, either method can provide a preliminary test result to judge whether the tested material can be of PAF. This can reduce time and costs before conducting a further detailed investigation.

Arsenic concentration is highly elevated in the ore zone samples (Table 4; Figure 9) and is consistent with the EPMA results, confirming that it is predominantly present in the vein-located pyrite and galena minerals (Table 2; Figure 6). In contrast, a low concentration of As is found in the wall rock (both hanging wall and footwall zones) samples (Figure 9), and it is also evidenced in the low As content in the pyrites of the hanging wall zone (Table 2). Consequently, comparing these results suggests that the mineralized veins (or ores) are likely the primary source of As in the Chatree mine. However, Chotpantarat et al. [47] reported that As in the tailing materials is under detection level, and Changul et al. [13] found that tailing materials are classified as NAF (Figure 7a).

In contradiction to As, this study reveals that Mn has multiple sources at the Chatree mine, as it is elevated and can be sourced from both vein and wall rocks in the hanging wall zone (Figure 9). Our petrographic and EPMA results found that Mn-rich carbonate (i.e., calcite) is commonly present in veins as a gangue mineral (Figure 6), and the Mn contents present in the hanging wall zone come from the contamination of veinlets (Figure 3g). The carbonate is classified as calcite (avg. formula: $Ca_{0.987}Mg_{0.005}Fe_{0.000}Mn_{0.017}CO_3$). Calcite containing Mn in its crystal structures will be salt and dissolve in an acid solution [63]. Mn can partition from the calcite structure and contaminate into the environment. This is consistent with higher Mn levels compared with other trace metals in groundwater monitoring wells [8]. Of these, Mn in the hanging wall zone is more environmentally concerned, as the lithic-rich fiamme breccia rocks of the hanging wall zone are characterized predominantly as PAF material (Figure 7). The Mn in the ore zone also contains a potential risk, and it is reported by Changul et al. [13] that Mn content in the tailing materials is high (2028 ppm on average), exceeding the Thai standard of Habitat and Agriculture (1800 ppm). Mn-bearing calcites may be the main source of Mn, which is the most leached metal and the most mobility metal from soil tailings [8,13]. However, such Mn levels are not distinctly high, as typical igneous rocks have Mn ranging from 450 to 1800 ppm [43–46]. The Mn content range of the typical igneous rocks is more or less similar to the ranges of the ore and hanging wall zones (Table 4; Figure 9); therefore, the Mn contents in the rocks at the H ore lens are indicated to be common background values.

6. Conclusions

This study conducted a mineral and geochemical investigation of the H-pit of the Chatree mine to assess the ARD potential and sources of heavy metals in the ore and host

rocks, with a specific focus on the link between the collected results of environmental aspects and field geology information to identify the sources. As a result, the following key conclusions can be drawn from this study:

(1). Au-Ag mineralization at the H ore lens occurs as veins/veinlets with minor breccias and is composed of quartz-carbonate-chlorite-sulfide-electrum veins. They are selectively hosted in the polymictic mafic-intermediate breccia in the host volcanic rock succession, which can be distinctly classified into footwall, ore, and hanging wall zones.

(2). The mineralized veins are chiefly characterized by open space-filling banded textures and abundant base metal sulfides, including pyrite, chalcopyrite, galena, and sphalerite. Such mineralization characteristics at the H ore lens are compatible with the deeper part of the low-sulfidation epithermal system.

(3). The ABA and NGA test results reveal that the lithic-rich fiamme breccia unit in the hanging wall zone is classified as PAF rock, caused by abundant disseminated pyrites in the unit forming due to hydrothermal alteration during the mineralizing event.

(4). The ore material has high contents of As, Cd, Cu, Pb, and Zn compared to the values in the hanging and footwall samples, but Mn content is similar between the ore, hanging wall, and footwall samples. As, Cd, and Zn are in the ore zone, hanging walls and footwalls are higher than typical igneous rocks, whereas Cr, Mn, and Ni are in the range of general igneous rocks. The sources of Cu, Pb, and Zn should originate predominantly from chalcopyrite, galena, and sphalerite, respectively. Other heavy metals (e.g., As, and Cd) mainly occur as trace elements in sulfide minerals, particularly in galena, pyrite, and sphalerite. Mn is indicated to occur as Mn-rich calcite.

(5). This study was conducted using drill hole data and cores created during the exploration program at the Chatree deposit. It was demonstrated that a detailed and comprehensive understanding of the geological, geochemical, and mineralization characteristics of this deposit, even in the early exploration stage, is useful for predicting any potential environmental impacts in the future.

References

1. Dold, B. Acid rock drainage prediction: A critical review. *J. Geichem. Explor.* **2017**, *172*, 120–132.
2. Hamdani, A.H.; Hutabarat, J.; Haryanto, A.D. The Acid-Base Accounting (ABA) of Overburden Rock to Predict Acid Mine Water in Kasai Coal Mining, Indonesia. *Orient. J. Chem.* **2019**, *35*, 1103–1111.
3. Parbhakar-Fox, A.; Lottermoser, B.G. A critical review of acid rock drainage prediction methods and practices. *Miner. Eng.* **2015**, *82*, 107–124.
4. Smart, R.; Skinner, W.; Levay, G.; Gerson, A.; Thomas, J.; Sobieraj, H.; Schumann, R.; Weisener, C.; Weber, P.; Miller, S. *ARD Test Handbook: Project P387A, Prediction and Kinetic Control of Acid Mine Drainage*; AMIRA, International Ltd.: Melbourne, Australia; Ian Wark Research Institute: Melbourne, Australia, 2002; p. 41.
5. Stewart, W.A.; Miller, S.D.; Smart, R. Advances in Acid Rock Drainage (ARD). In Proceedings of the 7th International Conference on Acid Rock Drainage (ICARD), St. Louis, MO, USA, 26–30 March 2006; pp. 2098–2119.
6. John, D.A.; Vikre, P.G.; du Bray, E.A.; Blakely, R.J.; Fey, D.L.; Rockwell, B.W.; Mauk, J.L.; Anderson, E.D.; Graybeal, F.T. *Descriptive Models for Epithermal Gold-Silver Deposits*; U.S. Geological Survey: Reston, VA, USA, 2018; Volume 247.
7. Assawincharoenkij, T.; Hauzenberger, C.; Sutthirat, C. Mineralogy and geochemistry of tailings from a gold mine in northeastern Thailand. *Hum. Ecol. Risk Assess.* **2017**, *23*, 364–387.
8. Chotpantarat, S.; Chunhacherdchai, L.; Wikiniyadhanee, R.; Tongcumpou, C. Effects of humic acid amendment on the mobility of heavy metals (Co, Cu, Cr, Mn, Ni, Pb, and Zn) in gold mine tailings in Thailand. *Arab. J. Geosci.* **2015**, *8*, 7589–7600.
9. Fashola, M.O.; Ngole-Jeme, V.M.; Babalola, O.O. Heavy metal pollution from gold mines: Environmental effects and bacterial strategies for resistance. *Int. J. Environ. Res. Public Health* **2016**, *13*, 1047.
10. Lottermoser, B.G. Introduction to mine wastes. In *Mine Wastes*; Springer: Berlin/Heidelberg, Germany, 2010; pp. 1–41.
11. Parbhakar-Fox, A.K.; Edraki, M.; Walters, S.; Bradshaw, D. Development of a textural index for the prediction of acid rock drainage. *Miner. Eng.* **2011**, *24*, 1277–1287.
12. Kingsgate. *Kingsgate Mineral Resources and Ore Reserves 2016*; ASX Online; ASX: Sydney, Australia, 2016; p. 16.
13. Changul, C.; Sutthirat, C.; Padmanahban, G.; Tongcumpou, C. Chemical characteristics and acid drainage assessment of mine tailings from Akara Gold mine in Thailand. *Environ. Earth Sci.* **2010**, *60*, 1583–1595.
14. Changul, C.; Sutthirat, C.; Padmanahban, G.; Tongcumpou, C. Assessing the acidic potential of waste rock in the Akara gold mine, Thailand. *Environ. Earth Sci.* **2010**, *60*, 1065–1071.
15. Chotpantarat, S. A review of static tests and recent studies. *Am. J. Appl. Sci.* **2011**, *8*, 400.
16. Sutthirat, C. Geochemical application for environmental monitoring and metal mining management. In *Environmental Monitoring*; Ekundayo, E., Ed.; InTechOpen: London, UK, 2011; pp. 91–108.
17. Sutthirat, C.; Changul, C. Geochemical characteristics of waste rocks from the Akara gold mine, Phichit Province, Thailand. *Arab. J. Sci. Eng.* **2013**, *38*, 135–147.
18. Metcalfe, I. Stratigraphy, paleontology and paleogeography of the Carboniferous of Southeast Asia. *Mém. Soc. Géol. Fr.* **1984**, *147*, 107–118.
19. Metcalfe, I. Late Palaeozoic and Mesozoic tectonic and palaeogeographical evolution of SE Asia. *Geol. Soc. Spec. Publ.* **2009**, *315*, 7–23.
20. Sone, M.; Metcalfe, I. Parallel Tethyan sutures in mainland Southeast Asia: New insights for Palaeo-Tethys closure and implications for the Indosinian orogeny. *C. R. Geosci.* **2008**, *340*, 166–179.
21. Zaw, K.; Meffre, S.; Lai, C.-K.; Burrett, C.; Santosh, M.; Graham, I.; Manaka, T.; Salam, A.; Kamvong, T.; Cromie, P. Tectonics and metallogeny of mainland Southeast Asia—A review and contribution. *Gondwana Res.* **2014**, *26*, 5–30.
22. Bunopas, S.; Vella, P. Tectonic and geologic evolution of Thailand. In Proceedings of the A Workshop on Stratigraphic Correlation of Thailand and Malaysia, Haad Yai, Thailand, 8–10 September 1983.
23. Kamvong, T.; Zaw, K.; Meffre, S.; Maas, R.; Stein, H.; Lai, C.-K. Adakites in the Truong Son and Loei fold belts, Thailand and Laos: Genesis and implications for geodynamics and metallogeny. *Gondwana Res.* **2014**, *26*, 165–184.
24. Kamvong, T.; Zaw, K. The origin and evolution of skarn-forming fluids from the Phu Lon deposit, northern Loei Fold Belt, Thailand: Evidence from fluid inclusion and sulfur isotope studies. *J. Asian Earth Sci.* **2009**, *34*, 624–633.
25. Khositanont, S. Gold and Iron–Gold Mineralization in the Sukhothai and Loei–Phetchabun Fold Belts. Ph.D. Thesis, Chiang Mai University, Chiang Mai, Thailand, 2008.
26. Rodmanee, T. Genetic Model of Phu Thab Fah Gold Deposit Ban Huai Phuk Amphoe Wang Saphung Changwat Loei. Master's Thesis, Chiang Mai University, Chiang Mai, Thailand, 2000.
27. Zaw, K.; Meffre, S. *Metallogenic Relations and Deposit Scale Studies, Final Report: Geochronology, Metallogenesis and Deposit Styles of Loei Fold Belt in Thailand and Laos PDR*; University of Tasmania: Hobart, Austrialia, 2007.
28. Kaewpaluk, S.; Salam, A.; Assawincharoenkij, T.; Manaka, T.; Poompuang, S.; Munsamai, S. Geology, mineralization, and alteration of B Prospect of the epithermal Au-Ag deposit in Central Thailand: A study on Chatree's satellite deposit for future gold exploration. *Sci. Asia* **2022**, *49*, 131–140.
29. Rongkhapimonpong, P. Characteristics of Vein Related to High Grade Gold Mineralization from Eastern A Pit of the Chatree Gold Deposit, Changwat Phichit and Phetchabun. Master's Thesis, Chulalongkorn University, Bangkok, Thailand, 2015.
30. Salam, A. A Geological, Geochemical and Metallogenic Study of the Chatree Epithermal Deposit, Phetchabun Province, Central Thailand. Ph.D. Thesis, University of Tasmania, Hobart, Australia, 2013.

31. Salam, A.; Zaw, K.; Meffre, S.; McPhie, J.; Lai, C.-K. Geochemistry and geochronology of the Chatree epithermal gold–silver deposit: Implications for the tectonic setting of the Loei Fold Belt, central Thailand. *Gondwana Res.* **2014**, *26*, 198–217.

32. Tangwattananukul, L.; Ishiyama, D. Characteristics of Cu-Mo Mineralization in the Chatree Mining Area, Central Thailand. *Resour. Geol.* **2018**, *68*, 83–92.

33. Tangwattananukul, L.; Ishiyama, D.; Matsubaya, O.; Mizuta, T.; Charusiri, P.; Sato, H.; Sera, K. Characteristics of Triassic epithermal Au mineralization at the Q prospect, Chatree mining area, Central Thailand. *Resour. Geol.* **2014**, *64*, 167–181.

34. Andrianarimanana, M.; Salam, A.; Sutthirat, C.; Manaka, T. Mineralogy and Petrography of Skarn in Khao Lek Area, Nong Bua District, Nakhon Sawan Province, Northern Thailand. *Bull. Earth Sci. Thail.* **2016**, *8*, 61–67.

35. Muller, C. Geochemistry, Fluid Characteristics and Evolution of the French Mine Gold Skarn System, Eastern Thailand. Bachelor's Thesis, University of Tasmania, Hobart, Australia, 1999.

36. Gemell Mining Engineers. *Technical Review of the Chatree Gold Project*; Gemell Mining Services Proprietary Limited: Sydney, Australia, 2013; Volume 53.

37. Bellenberg, S.; Buetti-Dinh, A.; Galli, V.; Ilie, O.; Herold, M.; Christel, S.; Boretska, M.; Pivkin, I.V.; Wilmes, P.; Sand, W. Automated microscopic analysis of metal sulfide colonization by acidophilic microorganisms. *Appl. Environ. Microbiol.* **2018**, *84*, e01835-18.

38. White, W.W., III; Lapakko, K.A.; Cox, R.L.; Plumlee, G.S.; Logsdon, M.J.; Filipek, L.F. Static-Test Methods Most Commonly Used to Predict Acid-Mine Drainage: Practical Guidelines for Use and Interpretation. In *The Environmental Geochemistry of Mineral Deposits: Part A: Processes, Techniques, and Health Issues Part B: Case Studies and Research Topics*; Society of Economic Geologists: Littleton, CO, USA, 1997; Volume 6, pp. 325–338.

39. Lei, L.; Watkins, R. Acid drainage reassessment of mining tailings, Black Swan nickel mine, Kalgoorlie, Western Australia. *Appl. Geochem.* **2005**, *20*, 661–667.

40. Weber, P.A.; Thomas, J.E.; Skinner, W.M.; Smart, R.S.C. A methodology to determine the acid-neutralization capacity of rock samples. *Can. Mineral.* **2005**, *43*, 1183–1192.

41. Weber, P.A.; Thomas, J.; Skinner, W.; Smart, R.S.C. Improved acid neutralisation capacity assessment of iron carbonates by titration and theoretical calculation. *Appl. Geochem.* **2004**, *19*, 687–694.

42. Price, W.A. *Draft Guidelines and Recommended Methods for the Prediction of Metal Leaching and Acid rock Drainage at Minesites in British Columbia*; BC Ministry of Employment and Investment: Smithers, BC, Canada, 1997; p. 141.

43. Bradl, H. Sources and origins of heavy metals. In *Interface Science and Technology*; Elsevier: Amsterdam, The Netherlands, 2005; pp. 1–27.

44. Turekian, K.K.; Wedepohl, K.H. Distribution of the elements in some major units of the earth's crust. *Geol. Soc. Am. Bull.* **1961**, *72*, 175–192.

45. Taylor, S. Geochemistry of andesites. In *Origin and Distribution of the Elements*; Elsevier: Amsterdam, The Netherlands, 1968; pp. 559–583.

46. Taylor, S.; White, A. Trace element abundances in andesites. *Bull. Volcanol.* **1966**, *29*, 177–194.

47. Chotpantarat, S.; Ong, S.K.; Sutthirat, C.; Osathaphan, K. Heavy metal contamination of groundwater and surrounding soils by tailing leachates from a gold mine in Thailand. *J. Sci. Res.* **2008**, *33*, 101–112.

48. Browne, P. Hydrothermal alteration in active geothermal fields. *Annu. Rev. Earth Planet. Sci.* **1978**, *6*, 229–248.

49. Einaudi, M.T.; Hedenquist, J.W.; Inan, E.E.; Simmons, S.F.; Graham, I. Sulfidation State of Fluids in Active and Extinct Hydrothermal Systems: Transitions from Porphyry to Epithermal Environments. In *Volcanic, Geothermal, and Ore-Forming Fluids: Rulers and Witnesses of Processes within the Earth*; Society of Economic Geologists: Littleton, CO, USA, 2005; Volume 10, p. 343

50. Camprubí, A.; Cardellach, E.; Canals, À.; Lucchini, R.; Albinson, T.; Nelson, C.E. The La Guitarra Ag-Au Low-Sulfidation Epithermal Deposit, Temascaltepec District, Mexico: Fluid Inclusion and Stable Isotope Data. In *New Mines and Discoveries in Mexico and Central America*; Society of Economic Geologists: Littleton, CO, USA, 2001; Volume 8, pp. 159–185.

51. Vikre, P.G. Precious metal vein systems in the National District, Humboldt County, Nevada. *Econ. Geol.* **1985**, *80*, 360–393.

52. Akcil, A.; Koldas, S. Acid Mine Drainage (AMD): Causes, treatment and case studies. *J. Clean. Prod.* **2006**, *14*, 1139–1145.

53. Lottermoser, B.G. Sulfidic mine wastes. In *Mine Wastes*; Springer: Berlin/Heidelberg, Germany, 2010; pp. 43–117.

54. Zhu, Y.; An, F.; Tan, J. Geochemistry of hydrothermal gold deposits: A review. *Geosci. Front.* **2011**, *2*, 367–374.

55. Simpson, M.P.; Mauk, J.L. Hydrothermal alteration and veins at the epithermal Au-Ag deposits and prospects of the Waitekauri area, Hauraki goldfield, New Zealand. *Econ. Geol.* **2011**, *106*, 945–973.

56. Hazarika, P.; Mishra, B.; Pruseth, K.L. Trace-element geochemistry of pyrite and arsenopyrite: Ore genetic implications for late Archean orogenic gold deposits in southern India. *Mineral. Mag.* **2017**, *81*, 661–678.

57. Koglin, N.; Frimmel, H.E.; Lawrie Minter, W.E.; Brätz, H. Trace-element characteristics of different pyrite types in Mesoarchaean to Palaeoproterozoic placer deposits. *Miner. Depos.* **2009**, *45*, 259–280.

58. Large, R.R.; Danyushevsky, L.; Hollit, C.; Maslennikov, V.; Meffre, S.; Gilbert, S.; Bull, S.; Scott, R.; Emsbo, P.; Thomas, H. Gold and trace element zonation in pyrite using a laser imaging technique: Implications for the timing of gold in orogenic and Carlinstyle sediment-hosted deposits. *Econ. Geol.* **2009**, *104*, 635–668.

59. Abraitis, P.; Pattrick, R.; Vaughan, D. Variations in the compositional, textural and electrical properties of natural pyrite: A review. *Int. J. Miner. Process.* **2004**, *74*, 41–59.

60. Huston, D.L.; Sie, S.H.; Suter, G.F.; Cooke, D.R.; Both, R.A. Trace elements in sulfide minerals from eastern Australian volcanic-hosted massive sulfide deposits; Part I, Proton microprobe analyses of pyrite, chalcopyrite, and sphalerite, and Part II, Selenium

levels in pyrite; comparison with delta 34 S values and implications for the source of sulfur in volcanogenic hydrothermal systems. *Econ. Geol.* **1995**, *90*, 1167–1196.

61. Van Ryt, M.; Sanislav, I.; Dirks, P.; Huizenga, J. Trace element associations in magnetite and hydrothermal pyrite from the Geita Hill gold deposit, Tanzania. *J. Geochem. Explor.* **2020**, *209*, 106418.
62. George, L.; Cook, N.J.; Ciobanu, C.L.; Wade, B.P. Trace and minor elements in galena: A reconnaissance LA-ICP-MS study. *Am. Mineral.* **2015**, *100*, 548–569.
63. Lund, K.; Fogler, H.S.; McCune, C.C.; Ault, J.W. Acidization—II. The dissolution of calcite in hydrochloric acid. *Chem. Eng. Sci.* **1975**, *30*, 825–835.